Advanced Aluminum Alloy Development and In Situ Fitness-for-Service Testing for Automotive Lightweighting

Dimitry Sediako, David Weiss, and Ahmed Nabawy

Abstract

Lightweighting has led to an increased use of aluminum alloys in many automotive systems, including the powertrain, body-in-white, and suspension. Fitness-for-service certification of new alloys for these applications frequently requires development of new testing methods that would subject the test components to realistic conditions of temperature and load, while studying the long-term materials' response. As the typical lifetime of a vehicle exceeds 3000 h, the new testing methods must provide clear indication on the material's suitability for a target application over a more realistic timeframe. An in situ study of the creep behavior using neutron diffraction quickly reveals the response of individual crystallographic planes to the applied load under the in-service operating conditions, yielding the critical information on the expected lifetime of the targeted component. This knowledge helps to identify alloy chemistry and processing conditions that result in manufacturing components capable of sustaining the thermal mechanical loads over the expected life cycle of a vehicle. Two advanced aluminum alloys, based on Al–Si and Al–Cu systems, have been the focus of this research.

Introduction

The present study was to explore the creep behavior of the aluminum 206 cast alloy by applying an in situ neutron-diffraction analysis. The main focus of the research was optimizing the performance of the alloy at high-temperatures, ranging from 200 to 250 °C, and determine the operative creep mechanisms in this alloy. The results not only explain the creep response of the 206 cast alloy, but they also contribute to understanding the creep behavior of the 200 series alloys in general. The creep data obtained in this study were also compared with creep data from Al–Si alloy. The present study can become a prototype of fitness-for-service certification for new industrial alloys and applications that require enhanced strength and creep resistance at elevated temperatures.

Creep test samples were machined from T7 heat-treated cast bars of aluminum 206 alloy, containing 4.5wt%Cu, 0.3wt%Mn, 0.25wt%Mg, and 0.22wt%Ti, that was supplied by ECK Industries Inc. The machined samples were stabilized in air at target temperatures of 200, 225, and 250 °C for at least 200 h before loading at the test temperatures.

Figure 1 depicts the experimental setup for in situ creep testing at the L3 beamline installed at the NRU research reactor of the Canadian Nuclear Laboratories, located in Chalk River, Ontario. This setup was also used in our earlier study [1]; it allows for simultaneous measurement of the elastic component of strain, using the neutron diffraction peak-shift method, as well as over-all strains that result from thermal expansion and plastic-elastic deformation measured by a high precision extensometer. The longitudinal axis of the sample was positioned parallel to the scattering vector, so the strains are measured parallel to the applied tensile stress for the selected crystallographic reflections of {111}, {311}, {200}, {220} and {222} planes. A one-dimensional

D. Sediako (✉) · A. Nabawy
Canadian Nuclear Laboratories, Chalk River, ON, Canada
e-mail: dimitry.sediako@cnl.ca

D. Weiss
ECK Industries Inc., Manitowoc, WI, USA

K.N. Solanki et al. (eds.), *Magnesium Technology 2017*,
The Minerals, Metals & Materials Series, DOI 10.1007/978-3-319-52392-7_88

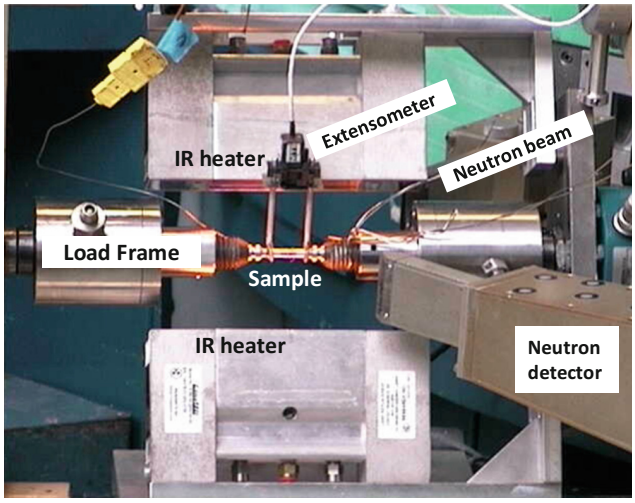

Fig. 1 Experimental setup for in-situ creep testing at the L3 beamline, Canadian Nuclear Laboratories

32-wire detector was used in this experiment, covering 3.2° of the diffraction angle for each of the measurements. A monochromatic neutron beam with a wavelength (λ) of 1.55 Å was used to monitor the change in the angular positions $\Delta(2\theta)$ of the neutron peaks produced by diffraction from the crystallographic planes. Lattice strain ε at a given reflection is then expressed as an observed change in the lattice spacing (1) and the lattice spacing was calculated using Bragg's law (2), as described in more details in [1].

$$\varepsilon = (d_0 - d)/d_0; \tag{1}$$

$$n\lambda = 2d\sin(\theta), \tag{2}$$

As the sample is heated to the required temperature, the change in diffraction angles for the targeted *hkl* reflections is measured by neutron diffraction to monitor the change in the lattice spacing associated with thermal expansion. A tensile load, about 80% of the yield strength of the alloy at the given temperature, is then applied. The load is maintained through the primary creep stage and during the first ~14 h of the steady state creep, and then the load is released for 1–2 h. The sample is then re-loaded again with an additional ~20 MPa stress, until the sample fails. Thus, at the three temperatures of 200, 225, and 250 °C, the ranges of applied stress were 137–196, 80–140, and 59–125 MPa, respectively.

During loading and reloading, the angular positions of the selected neutron diffraction peaks were continuously measured to study the evolution of the elastic lattice strains during the creep deformation, while the extensometer output —also continuously measured—represented the over-all strain experienced by the sample. The reference value for the lattice spacing was also periodically measured by neutron diffraction for the un-stressed (unloaded) condition prior to each loading stage.

Results and Discussion

The creep curves generated by the extensometer during the experiments are shown in Fig. 2. The governing power-law equation used in this analysis is expressed as:

$$\dot{\varepsilon} = A_0\sigma^n \exp\left(-\frac{Q}{RT}\right), \tag{3}$$

where $\dot{\varepsilon}$ is the minimum creep rate, 1/s; A_0 is dimensionless constant, σ is the applied stress, MPa, Q is the creep activation energy, kJ/mol; R is the universal gas constant, J/(mol K); and T is the absolute temperature, K.

In Fig. 3, the minimum strain rates (the steady-state or secondary creep rate) are plotted against the applied stresses, while also displaying the relevant stress exponent, n, and the corresponding activation energies, Q, between the three test temperatures. These figures represent the performance (creep response) of the 206 alloy at the applied loads and the temperature ranges that simulate the actual in-service conditions.

The high value of n indicates an accelerated creep deformation due to the increase in applied stress, as presented in the following equation:

$$n = \ln\left(\frac{\dot{\varepsilon}1}{\dot{\varepsilon}2}\right) / \ln\left(\frac{\sigma 1}{\sigma 2}\right) \tag{4}$$

For example, the n value of 34 at 225 °C indicates that the creep strain rate increases by ~200 times as the stress level increases from 120 to 140 MPa. However, the creep strain rate increases by just 3 times as the applied stress increases from 80 to 100 MPa at the same temperature, giving n of 5. Thus, for a reliable performance of a cast component at the temperature of 225 °C, the acting stress should be kept below 120 MPa while in-service.

With respect to the n values, during testing for fitness-for-service certification, the creep response of the 206 alloy should be analysed separately at three different levels of n; namely, for low ($n \ll 5$), medium ($n \sim 5$), and high ($n \gg 5$). These three distinct regions indicate the presence of three active creep mechanisms, which were discussed in details in a previous study on high temperature creep in Al–Si alloys [1]. It is apparent that the high sensitivity of the 206 alloy towards the applied stress level should be taken into account during the engineering design of the final product.

Activation energy represents the role of temperature in creep response of the alloy. The values of activation energy presented in Fig. 3 fall in two levels: 80–110 and 310 kJ/mol.

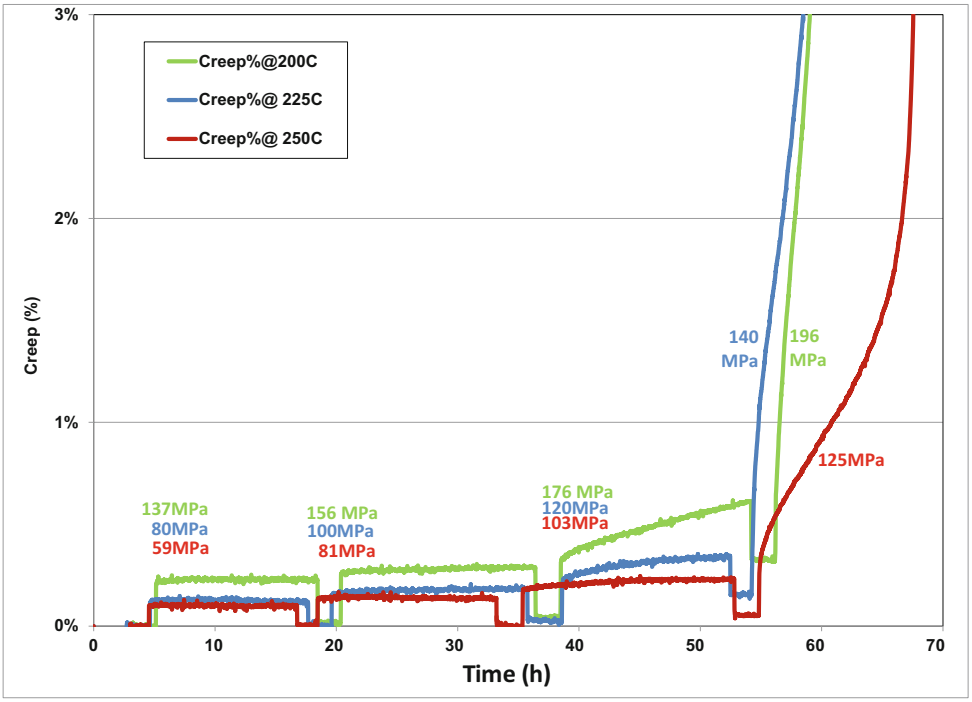

Fig. 2 Creep curves of the 206 alloy at different levels applied stresses and temperatures

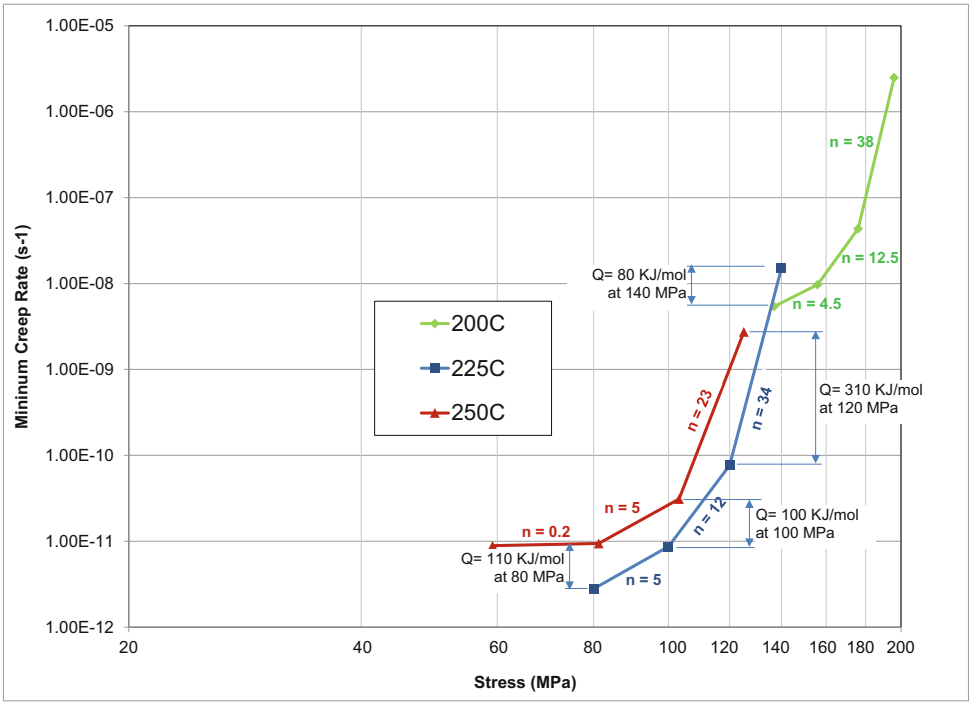

Fig. 3 Minimum creep rate of A206 alloy plotted versus the applied tensile stress

Figure 3 indicates, for example, that the creep rate increases by 3 times as the temperature increases from 225 to 250 °C at applied stress level of about 80 MPa. However, at the applied stress of 120 MPa, the creep rate increases by 36 times when the temperature increases from 225 to 250 °C. Therefore, the creep rates of the 206 alloy are likely controlled by dislocation core diffusion at the lower activation energy range (80–110 kJ/mol), and the cross-slip mechanism at the higher activation energy (310 kJ/mol). As the 206 alloy is a precipitation-hardened alloy, it is believed that the creep behavior of the alloy is significantly affected by the interaction between the dislocations and the hardening precipitates.

Neutron diffraction analysis has been applied to explore the relation between the macroscopic creep behavior and the

lattice strain evolution during the in situ creep test of the 206 alloy. The results obtained on the lattice strains for (111), (311), (220), (200), and (222) planes are presented in Fig. 4.

Anisotropy of the elastic properties for different *hkl* directions of the fcc structure is known and well reported in technical literature [2, 3]. However, the reported differences in, for example, modulus of elasticity are not excessively large and the deviations typically do not exceed 1–5% of the "bulk" value. The observed large differences in strain magnitude indicate partitioning in load distribution and dependent on acting creep mechanisms. The evolution of the lattice strains contributes to the understanding of the acting

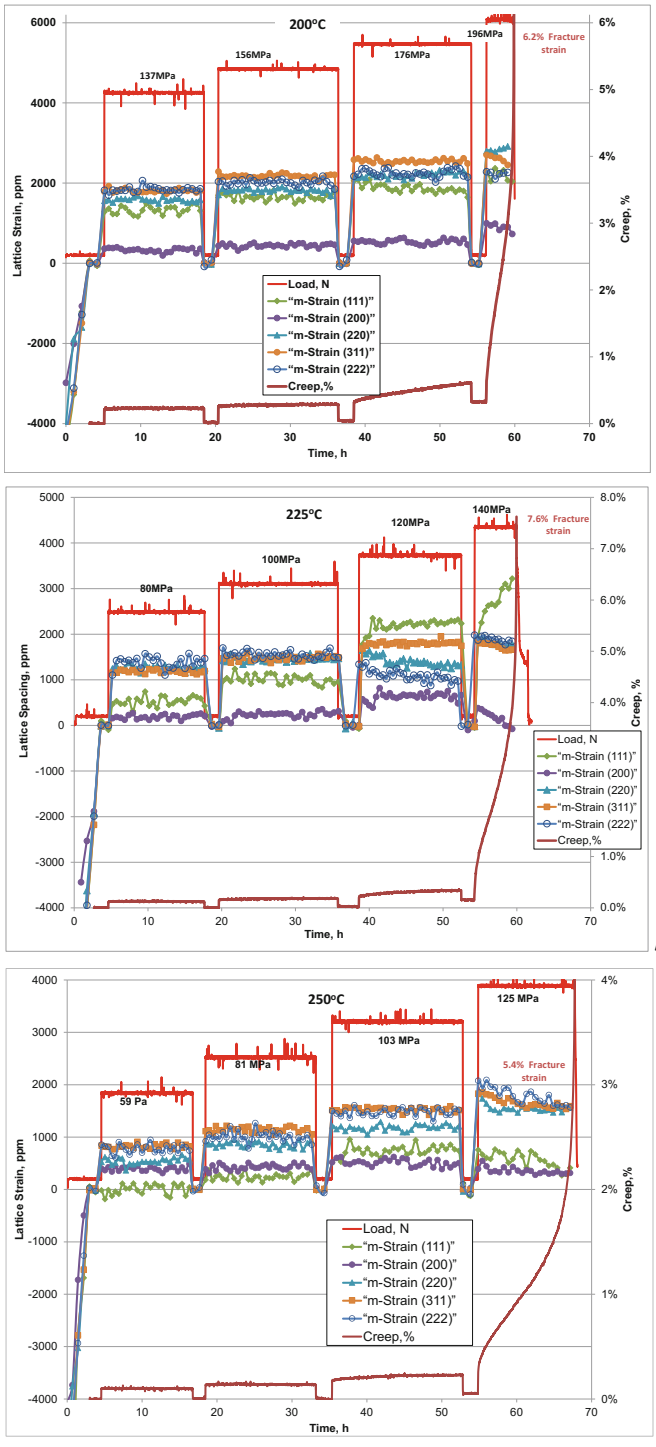

Fig. 4 Creep strain (%) and elastic microstrain (ppm) evolution at selected *hkl* planes at 200 °C **a**, 225 °C **b**, and 250 °C **c** during ascending cyclic loading for 206 alloy

creep mechanism because it reveals properties such as the dislocation mobility and density, cross-slipping planes and directions, and hardening and softening behavior. The first example is that the (200) plane typically displayed the lowest lattice strains at all of the applied stresses and temperatures, likely due to an active dislocation movement on this plane. Because the dislocation movement is a form of plastic deformation, it does not result in a direct increase of elastic strain. On the other hand, the (311), (220), and (222) planes typically exhibit the highest strains, indicating that the applied tensile load is supported by these planes to a large degree. The dislocation movements, therefore, are inhibited in these directions, possibly due to the presence of stable secondary intermetallic phases that restrict the dislocations.

Second, at the lower test temperature of 200 °C, most of the *hkl* planes tested, with exception of the (200) plane, contributed comparably to supporting the applied load. As the test temperature was increased to 225 °C, the contribution by the (111) plane became sporadic, and then much reduced at 250 °C.

A higher level of contribution in supporting the applied load by the (311) plane and a lower contribution of the (200) plane were also previously observed in a study [1] on Al–Si alloys. For example, Fig. 5 presents the results obtained in [1] on Al–7wt%Si alloy with dispersoid additions of 0.56%Zr, 0.2%Ti, and 0.3%V. In contrast with the results presented in Fig. 4 for the 206 alloy, the (111) plane for the Al–Si alloy contributed significantly to the strength of the material, because the elastic strains are typically the largest in this direction under all the conditions tested. Although the creep behaviour for both alloys is significantly affected by work hardening and by the interaction of the dislocations with the hardening precipitates, the observed difference in the (111) plane's contribution indicates that different creep dislocation mechanisms take place during tensile loading of Al–Cu and Al–Si alloys at elevated temperatures.

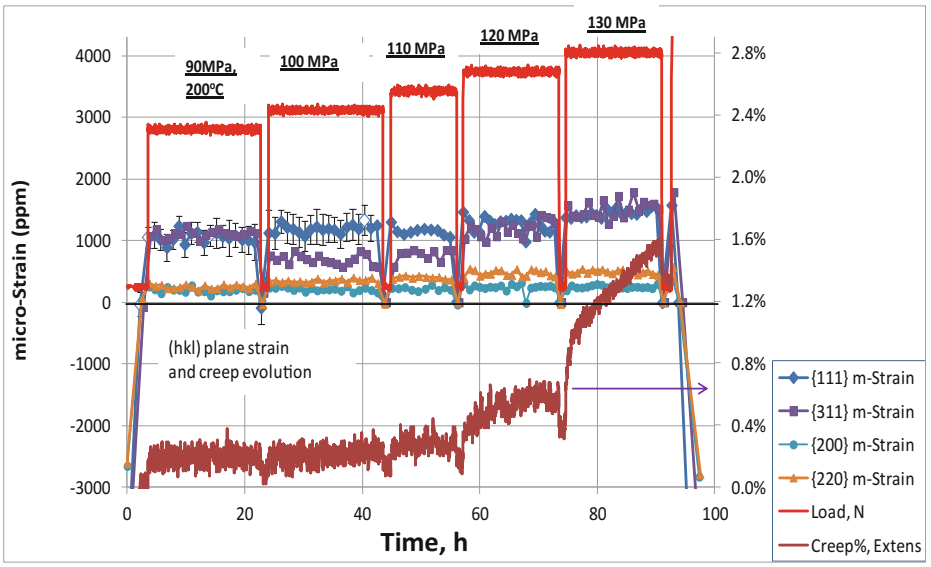

Fig. 5 Creep strain (%) and elastic microstrain (ppm) evolution at selected hkl planes at 200 °C **a** and 250 °C **b** during ascending cyclic loading for Al–Si alloy [1] with dispersoid additions of 0.56%Zr, 0.2%Ti, and 0.3%V

It was concluded in [1] that in Al–Si alloys, the crystallographic planes with lower packing density (e.g. 100, 110, 220) can be activated to carry more of the load, in some cases almost as much as the (111) plane. This activation was attributed to accumulated plastic deformation resulting in grain deformation that may lead to cross-slip from the (111) plane to the (311) and (220) planes. Similar deformation behavior was reported in a previous study [4], in which the cross-slip is activated from the (111) plane onto the (001) planes as the load increases.

The results obtained in this research on 206 Al–Cu alloy indicate that, as compared to the Al–Si data [1], the sample material exhibits a higher level of strength in the [311] and [220] crystallographic directions. As reported in previous studies [5–7], above 200 °C aluminum deforms easily by dislocation glide and many planes are thermally activated. Apparently, the thermally activated glide also played a role in the reduced contribution—i.e. reduced strength—of the {111} and {220} planes at 225 and 250 °C for the Al–Cu alloy. The load carrying capacity of the other *hkl* planes was sufficient to demonstrate the overall remarkable creep resistance of the 206 alloy under the tested conditions. For example, the tertiary creep stage for the 200 °C test was observed under the load of 196 MPa for the 206 alloy (supported by most of the measured planes, except {200}), whereas for the reinforced Al–7%Si alloy this creep stage was at stress below 140 MPa (supported mostly by the {111} and {311} planes). At 250 °C, the Al–Si alloy experienced the tertiary creep at just 88 MPa, while the load was supported by all the measured *hkl* planes. In contrast, the 206 alloy experienced the tertiary creep at higher stress of 125 MPa, even though {111} and {200} planes didn't register any significant strain.

Conclusions

1. The creep behavior of the 206 alloy is highly sensitive to the level of the applied stress. Three levels of the stress exponent (n) recorded in this study were low ($n \ll 5$), medium ($n \approx 5$), and high ($n \gg 5$), indicating three different creep mechanisms.
2. The results for the activation energy indicate that the creep rate of the 206 alloy is likely controlled by dislocation core diffusion at 80–110 kJ/mol, or cross-slip at 310 kJ/mol.
3. The (200) plane displays the lowest amount of the lattice strain at all applied stresses and temperatures, likely due to an active dislocation movement parallel to the [200] direction. The (311), (220), and (222) planes exhibited the highest level strains in this experiment, indicating a large contribution of these planes to supporting the applied load. The dislocation movements, therefore, are inhibited in these directions, likely due to the presence of stable secondary phases that restrict the movement of the dislocations.
4. A significant difference in the level of {111} strain was observed at 250 °C between the 206 alloy tested in this study and Al–Si alloy with dispersoid additions of Zr, Ti, and V, earlier studied in [1]. The thermally activated dislocation glide played a role in the reduced contribution —i.e. reduced strength—of the {111} and {220} planes at 225 and 250 °C for the Al–Cu alloy, whereas for the Al–Si alloy, all studied *hkl* planes contributed almost equally to supporting the applied load up to the transition to the tertiary creep.
5. In spite of the reduced contribution of {111} and {200} planes, the load carrying capacity of the other *hkl* planes, such as {311}, {220}, and {222} was sufficient to demonstrate the overall remarkable creep resistance of the 206 alloy under the tested conditions.

References

1. D. Sediako, W. Kasprzak, F. Czerwinski, A. Nabawy, A. Farkoosh, High temperature creep evolution in Al–Si alloys developed for automotive powertrain applications—a neutron in-situ study on hkl-plane creep response. Light Met. 2016 TMS-2016 (2016)
2. Z.L. Greer, Temperature, frequency, and young's modulus of an aluminum tuning fork. ISB J. Phys. (2011)
3. *Non-Destructive Testing—Standard Test Method for Determining Residual Stresses by Neutron Diffraction*. Technical Specification, ISO/TS 21432, ISO, 15 July 2005
4. J. Majimel, M.-J. Casanove, G. Molenat, A 2XXX aluminum alloy crept at medium temperature: role of thermal activation on dislocations mechanisms. Mater. Sci. Eng. A **380**, 110–116 (2004)
5. D. Caillard, J.L. Martin, Glide of dislocations in non-octahedral planes of FCC metals: a review. Int. J. Mater. Res. **100**(10), 1403–1410 (2009)
6. M. Carrard, J.L. Martin, Philos. Mag. A **56**, 391 (1987)
7. R. Le Hazif, P. Dorizzi, J.P. Poierier, Acta Met. **21**, 903 (1973)